Defence Research and Development Canada
Recherche et développement pour la défense Canada

CAN UNCLASSIFIED

The Empirical Canadian High Arctic Ionospheric Model (E-CHAIM)

Topside

David Themens

P.T. Jayachandran
Anthony McCaffrey
Benjamin Reid
University of New Brunswick

Prepared by:
University of New Brunswick
8 Bailey Drive
P.O. Box 4400
Fredericton (New Brunswick) E3B 5A3
Canada
PSPC Contract Number: W7714-186507/001/SS
Technical Authority: Thayananthan Thayaparan, Defence Scientist
Contractor's date of publication: March 2018

Defence Research and Development Canada
Contract Report
DRDC-RDDC-2018-C202
November 2018

Canada

IMPORTANT INFORMATIVE STATEMENTS

This document was reviewed for Controlled Goods by Defence Research and Development Canada using the Schedule to the *Defence Production Act*.

The Empirical Canadian High Arctic Ionospheric Model (E-CHAIM)

Topside

David R. Themens
University of New Brunswick

P.T. Jayachandran, Anthony M. McCaffrey, Benjamin Reid
University of New Brunswick

Prepared For:
Department of National Defence
DRDC-Ottawa, BLDG 29, 3701 Carling Ave.
Ottawa, Ontario, K1A0Z4, Canada
Contract # W7714-186507/001/SS

The following work is supported through the All Domain Situational Awareness (ADSA) Science & Technology program, contract number W7714-186507/001/SS.

Abstract

In this study, we present a topside model representation to be used by the Empirical Canadian High Arctic Ionospheric Model (E-CHAIM). In the process of this, we also present a comprehensive evaluation of the NeQuick's, and by extension the International Reference Ionosphere (IRI)'s, topside electron density model for mid and high latitudes in the northern hemisphere. Using data gathered from all available Incoherent Scatter Radars, Topside Sounders, and GNSS Radio Occultation satellites, we show that the current NeQuick parameterization sub-optimally represents the shape of the topside electron density profile at these latitudes and performs poorly in the representation of seasonal and solar cycle variations of the topside scale thickness. Despite this, the simple, one-variable, NeQuick model is a powerful tool for modeling the topside ionosphere. By refitting the parameters that define the maximum topside scale thickness and the rate of increase of the scale height within the NeQuick topside model function, r and g, respectively, as well as refitting the model's parameterization of the scale height at the F-region peak, Ho, we find considerable improvement in the NeQuick's ability to represent the topside shape and behaviour. Building on these results we present a new topside model extension of the E-CHAIM based on the revised NeQuick function. Overall RMS errors in topside electron density are improved over the traditional IRI/NeQuick topside by 31% for a new NeQuick parameterization and by 36% for a newly proposed topside for E-CHAIM.

Significance for Defence and Security

This work is a direct extension of the previous E-CHAIM NmF2 and hmF2 model components to reflect the electron density of the ionosphere above the F2-peak. While the development of the E-CHAIM topside mainly benefits GNSS positioning applications, a topside model is crucial to the later phases of the CHAIM project, which assimilate ground- and space-based GNSS observations to improve E-CHAIM's performance as a whole. An accurate topside model facilitates robust data assimilation of integrated electron density observations, such as those available from GNSS.

Résumé

Dans cette étude, nous présentons une représentation des couches supérieures qui pourra être utilisée par l'Empirical Canadian High Arctic Ionospheric Model (E-CHAIM), modèle empirique ionosphérique de l'Extrême-Arctique canadien. Dans le même élan, nous présentons aussi une évaluation approfondie du modèle de densité des électrons des couches supérieures NeQuick, et par extension de l'initiative International Reference Ionosphere (IRI), pour les latitudes moyennes à élevées dans l'hémisphère nord. Au moyen de données recueillies par tous les radars à diffusion incohérente, satellites de sondage en altitude et satellites de radio-occultation du GNSS disponibles, nous montrons que le paramétrage actuel de NeQuick représente de manière sous-optimale la forme du profil de densité des électrons des couches supérieures à ces latitudes et qu'elle représente médiocrement les variations saisonnières et liées au cycle solaire de l'épaisseur d'échelle en altitude. Malgré cela, le modèle NeQuick, simple et à variable unique, est un outil puissant pour modéliser la couche supérieure de l'ionosphère. En réajustant les paramètres qui définissent l'épaisseur d'échelle en altitude, et le taux d'augmentation de la hauteur d'échelle dans la fonction de modélisation de NeQuick, r et g, respectivement, ainsi qu'en réajustant le paramétrage du modèle pour la hauteur d'échelle au sommet de la région F, Ho, nous obtenons une nette amélioration de la capacité de NeQuick de représenter la forme et le comportement de la couche supérieure. En nous basant sur ces résultats, nous présentons une nouvelle extension du modèle pour les couches supérieures d'E-CHAIM, d'après la fonction révisée de NeQuick. Les erreurs quadratiques moyennes globales dans la densité des électrons de la couche supérieure sont améliorées par rapport au modèle traditionnel IRI/NeQuick, de 31 % pour un nouveau paramétrage de NeQuick, et de 36 % pour une nouvelle couche supérieure pour E-CHAIM.

Table of contents

Abstract……. i
Significance for Defence and Security i
Résumé……. ii
Importance pour la défense et la sécurité ..... **Error! Bookmark not defined.**
Table of contents iii
List of figures iv
List of tables vi
Acknowledgements vii
1 Introduction..... 1
2 Data 4
2.1 Incoherent Scatter Radar (ISR)..... 4
2.2 Radio Occultation (RO)..... 5
2.3 Topside Sounder..... 5
3 Limitations of the Current NeQuick Topside Model and its Parameterization 7
3.1 H_o parameterization 7
3.2 Does H_o need new parameters? 11
3.3 Topside Shape Errors 11
4 A Refitted and Parameterized NeQuick Topside..... 14
4.1 New r and g constants..... 14
4.2 Re-fitting H_o for a regional version of the traditional NeQuick 15
4.3 A Topside for E-CHAIM..... 18
5 Conclusion 20
References/Bibliography.... 21
List of symbols/abbreviations/acronyms/initialisms 24

List of figures

Figure 1. a) Plot of NeQuick scale height vs. altitude for the following r and g combinations (r,g): red (20,0.2024), black (100,0.125), blue (100,0.5), and green (100,1.0). Dotted lines represent the asymptotes for the corresponding curve. b) Plot of NeQuick scale height vs. altitude subsection of the domain presented in a), where dotted lines now represent the corresponding H = Ho + g(h-hmax) curve. 2

Figure 2. A map of the locations of the ISRs used in this study with measurement density from all data sources superimposed (density is presented in 2o x 2o latitude x longitude bins)..... 5

Figure 3. Plots of monthly median Ho derived from measurements (black), from the traditional IRI/NeQuick (red), and from refitting the NeQuick k parameterization (green) for 00LT, 06LT, 12LT, and 18LT local time hours..... 8

Figure 4. A) Plots of monthly RMS Ho errors for the traditional IRI/NeQuick (red) and for the refitted NeQuick k parameterization (green) for 00LT, 06LT, 12LT, and 18LT local time hours between 2007 and 2016. B) Same as Figure 3, but only for 2007-2016..... 9

Figure 5. a) Distributions of Ho differences from measurement-derived values for the traditional IRI/NeQuick (red) and the refitted k parameterization (black). b) Mean (solid) and standard deviation ranges (dashed) of Ho vs. geomagnetic latitude. c) Mean (solid) and standard deviation ranges (dashed) of Ho vs. magnetic local time. d) Mean (solid) and standard deviation ranges (dashed) of Ho vs. integrated AE index..... 10

Figure 6. Left) Normalized distributions of absolute electron density errors, as a percentage of NmF2, vs. altitude for the traditional IRI/NeQuick. Right) Normalized distributions of the corresponding relative errors in electron density vs altitude..... 12

Figure 7. Same as Figure 6 but for the best-fitted NeQuick parameterization (r,g) = (100,0.125). 13

Figure 8. Contour plots a) of the average NmF2-relative RMS error and b) the average correlation coefficient of best-fitted NeQuick profile functions using varying values of r and g. The + marks the corresponding minimum RMS or maximum correlation for each plot. The X marks the values used by the traditional NeQuick model..... 14

Figure 9. Same as Figure 6 but for the best-fitted new NeQuick model function using (r,g) = (20,0.2024). 15

Figure 10. Same as Figure 5 but the black curves now represent the new Ho parameterization of Equation 9 and the red curves represent the refitted traditional NeQuick k parameterization using the new (r,g) = (20,0.2024). 16

Figure 11. Same as Figure 6 but for the new NeQuick parameterization of Equation 9 with (r,g) = (20,0.2024). 17

Figure 12. Same as Figure 10 but for H0 derived from the E-CHAIM parameterization (black) and that of Equation 9 (red). 19

List of tables

Table 1. Summary of the characteristics of the topside sounder missions used in this study. 6

Acknowledgements

This paper is supported by Defense Research and Development Canada contract #W7714-186507/001/SS. PFISR and RISR operations are supported by NSF Cooperative Agreement AGS-1133009. ISR data was acquired through the use of the Madrigal data portal at http://isr.sri.com/madrigal/. We would like to thank all ISR operators for their continued contribution of data to the Madrigal Database. The authors acknowledge UCAR/CDAAC (Boulder, CO, USA) for the use of the CHAMP, GRACE, and COSMIC RO data. Intercosmos-19 topside sounding data was provided by IZMIRAN. EISCAT is an international association supported by research organisations in China (CRIRP), Finland (SA), Japan (NIPR and STEL), Norway (NFR), Sweden (VR), and the United Kingdom (NERC). The authors would also like to thank Dr. Bruno Nava for his insightful comments and suggestions regarding this manuscript and the following people for their contributions of data to this project:

Dieter Bilitza, George Mason University, Fairfax, Virginia

Philip J. Erickson, Haystack Observatory, Massachusetts Institute of Technology, Cambridge, Massachusetts, US

Ingemar Häggström, EISCAT Scientific Association, Kiruna, Sweden

Mykhaylo V. Lyashenko, Institute of Ionosphere, National Academy of Sciences of Ukraine and Ministry of Education and Science of Ukraine, Kharkiv, Ukraine

Roger H. Varney, SRI International, Menlo Park, California, US

Ljubov Pustovalova, Pushkov Institute of Terrestrial Magnetism, Ionosphere and Radio Wave Propagation (IZMIRAN), Moscow, Russia

1 Introduction

The current standard for topside specification within the International Reference Ionosphere (IRI) and NeQuick empirical electron density models is the NeQuick2 topside parameterization, given by the following set of functions

$$N(h) = \frac{4N_{max}}{(1+\exp(z))^2}\exp(z) \quad (1)$$

$$z = \frac{h-hmax}{H} \quad (2)$$

$$H = H_0\left[1 + \frac{rg(h-h_mF2)}{rH_0+g(h-h_mF2)}\right] \quad (3)$$

where N_{max} is the peak density of the layer, h is altitude, h_{max} is the height of the layer peak, H_o is the scale height at the layer peak, r = 100, and g = 0.125 [Nava et al., 2008; Coïsson et al., 2006]. This parameterization is a semi-Epstein layer function with a varying topside scale height given by Equation (3), where the scale height exhibits roughly linear behaviour near the F-region peak and asymptotic behaviour at several thousand kilometers above the F-region ppeak. While the IRI has two other topside options (IRI2001 and IRI2001-cor), the NeQuick option was recommended as the standard option based on an evaluation with Alouette and ISIS topside sounder data [Bilitza, 2009].

An illustration of the behaviour of the scale height function given by Equation (3) is provided in Figure 1. For a given H_o value, here chosen to be 60km for illustration purposes, the g parameter controls the rate of increase of the scale height near the F-region peak. To illustrate this, we have plotted dotted lines corresponding to $H = H_o+g(h-hmax)$ in Figure 1b. The r parameter controls the scale height at the asymptote, which is given by $H_{asymptote} = (r+1)H_o$. In Figure 1a, the asymptotes derived from this relationship are plotted as dotted lines.

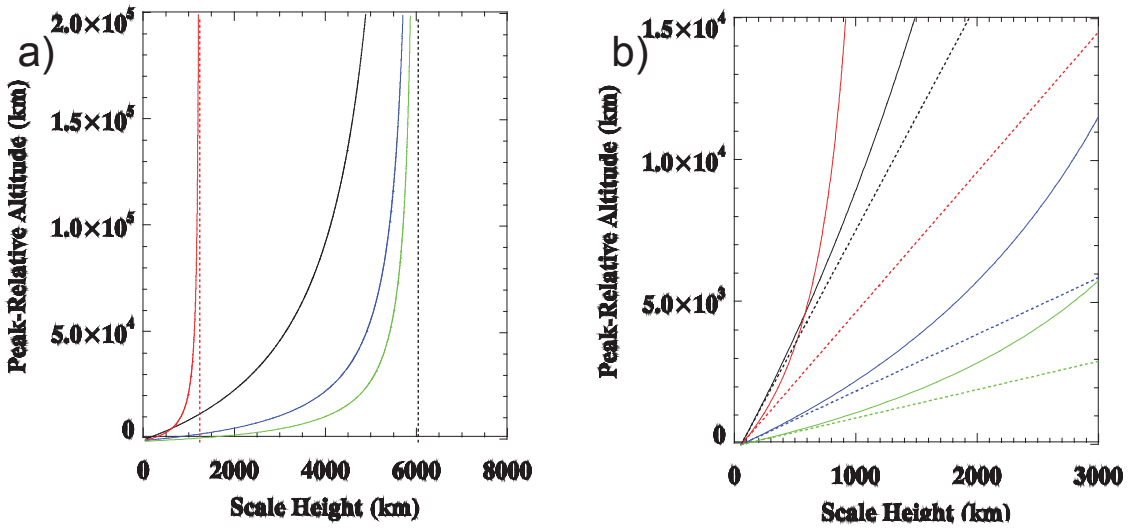

Figure 1. *a) Plot of NeQuick scale height vs. altitude for the following r and g combinations (r,g): red (20,0.2024), black (100,0.125), blue (100,0.5), and green (100,1.0). Dotted lines represent the asymptotes for the corresponding curve. b) Plot of NeQuick scale height vs. altitude subsection of the domain presented in a), where dotted lines now represent the corresponding H = Ho + g(h-hmax) curve.*

Unfortunately, the choice of r and g constants has never been explicitly discussed in the literature, even in the original study that proposed the current NeQuick parameterization (e.g. Equation 3) [Radicella and Leitinger, 2001]. Given the significant dependence of the topside model on the choice of these parameters, the lack of previous discussion regarding their significance, and the fact that the choice of these parameters has not changed since the original publication of the model (despite changes to Equation 3 over the

years), it is imperative that these parameters be adequately investigated if one wishes to properly evaluate and re-parameterize the NeQuick topside model.

For the IRI and NeQuick, the H_o parameter in Equation (3) is parameterized through the following relationships

$$H_0 = k \cdot B2Bot \qquad (4)$$

$$k = 3.22 - 0.0538foF2 - 0.00664hmF2 + 0.113\frac{hmF2}{B2_{Bot}} + 0.00257R12 \quad (5)$$

where foF2 is the peak critical frequency of the ionosphere, hmF2 is the peak height of the ionosphere, R12 is the 12-month smoothed sunspot number, and B2Bot is given by the following

$$B2_{Bot} = \frac{0.365NmF2}{(dN/dh)_{max}} \quad (6)$$

$$\ln\left(\left(\frac{dN}{dh}\right)_{max}\right) = -3.467 + 1.714\ln(foF2) + 2.02\ln(M(3000)F2) \qquad (7)$$

where M(3000)F2 is the transmission factor at 3000km (i.e. the ratio of the Maximum Usable Frequency (MUF) at a transmission distance of 3000km to foF2). The choice to parameterize Ho as a function of separate parameters, B2Bot and k, rather than directly parameterizing Ho, is originates from the original NeQuick topside model that used $H{=}k{\cdot}B2Bot$ and allowed for the simple calculation of the total electron content as a function of only NmF2, B2Bot, and k [Radicella and Zhang, 1995]. As this is no longer an necessary functionality of the model, a direct parameterization of Ho may be in order.

The need to reassess the NeQuick representation at upper-mid and high latitudes stems from recent studies that have shown appreciable issues with the NeQuick topside parameterization. For example, at high latitudes, Themens et al. [2014] show that the NeQuick parameterization struggled in the representation of topside thickness during the solar minimum between cycles 23 and 24. Themens and Jayachandran [2016] show that the errors in the IRI-generated topside thickness account for the majority of the errors in the IRI's representation of high latitude Total Electron Content (TEC). These errors were further verified by Incoherent Scatter Radar (ISR) observations at several polar cap and auroral oval locations [Bjoland et al., 2016; Themens et al., 2017b], where Themens et al. [2017b] relates these errors to several different limitations in the current NeQuick parameterization. In the sub-auroral trough region, Xiong et al. [2013] showed that the IRI overestimates near peak and lower-topside electron density by an average of 20%. Other, less localized studies, such as Zhu et al. [2015] and Gordiyenko and Yakovets [2017], have shown significant issues in the model at virtually all latitudes. These limitations highlight a need to develop a new topside thickness parameterization for use at mid and high latitudes.

This study explores the performance of the NeQuick topside parameterization in its use above 45^{o}N geomagnetic latitude using an unprecedented amount of topside observations and proposes a new parameterization of the model that could be used with the IRI and NeQuick as preparation for adopting the NeQuick as the topside representation in E-CHAIM. In Section 3, we first assess the main challenges that must be addressed if one is to re-parameterize the model for use at high and upper-mid latitudes, namely: 1) the limitations of the H_o parameterization in its ability to capture the variability of H_o, and 2) the limitations of the current topside function to capture the shape of the topside electron density profile. In Section 4.1, we address issue (2) by assessing the existing values of r and g and proposing new values. In Section 4.2, we re-fit the NeQuick parameterization of H_o, first in a manner that preserves the form of the original model and later in a new form. Finally, in Section 4.3, we build on the results of Sections 3 and 4.1 to present a proposed parameterization for the topside representation in the Empirical Canadian High Arctic Ionospheric Model (E-CHAIM) [Themens et al., 2017a].

2 Data

This study uses all available topside observations above 45°N geomagnetic latitude from several instruments including: Incoherent Scatter Radars (ISRs), GPS Radio Occultation (RO) satellites, and topside sounders.

2.1 Incoherent Scatter Radar (ISR)

ISR's are capable of estimating the electron density profile of the ionosphere from altitudes as low as the lower E-region and D-Region to well into the F-Region topside or even the lower plasmasphere. A full description of the methods used for estimating these electron densities can be found in Evans [1969].

For this study, ISR data was gathered from the Madrigal Database at http://isr.sri.com/madrigal/. Typically, this data has not been used for topside model representations due to its limited altitude coverage and limited spatial coverage. In this study, we are mainly concerned with the adjustment of the NeQuick model, which is a single parameter function requiring only the specification of the topside thickness H_0. The fact that this is a single parameter model allows us to make effective use of data with even limited vertical extent, assuming that the NeQuick function itself can adequately represent the curvature of the topside electron density profile. To make use of the ISR electron density profiles, we undertook the following procedure in order to ensure the quality of the dataset:

1) Data has been binned in altitude bins, with thicknesses ranging from 10km in the bottomside to 50km in the topside, over 15 minute intervals, using only data from beams above 45 degrees elevation.
2) Probability distribution functions are created for each bin and then fitted with a Gaussian to determine the electron density and standard deviation of the measurements in each bin.

This procedure is undertaken in order to account for the tendency of ISR measurements to exhibit a positive bias in statistical averages of low signal-to-noise measurements. In these situations, the distribution of electron density measurements in these bins is often artificially truncated at zero and thus a simple average would be positively biased when the density is smaller than the noise width of the measurements. Overall, this procedure resulted in the identification of 960,450 electron density profiles from between 1963 and 2016 for inclusion in the model fitting. The locations of the ISRs used in this study can be found in Figure 2, where ESR refers to the EISCAT Svalbard Radar, PFISR refers to the Poker Flat ISR, and RISR refers to the northern face of the Resolute ISR.

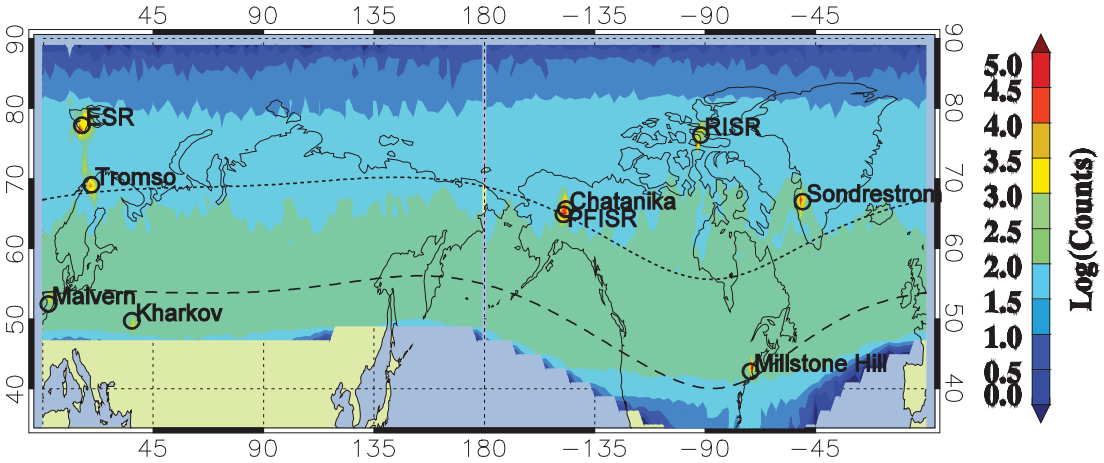

Figure 2. *A map of the locations of the ISRs used in this study with measurement density from all data sources superimposed (density is presented in 2o x 2o latitude x longitude bins).*

2.2 Radio Occultation (RO)

This study also makes use of RO electron density profiles from the Gravity Recovery and Climate Experiment (GRACE) and FORMOSAT-3/COSMIC missions. GRACE, a pair of satellites launched at an orbital altitude of 500km in the same 89° inclination orbital plane, has provided RO data between 2007 and 2016. COSMIC is a constellation of six Low Earth Orbit (LEO) satellites with orbital altitudes of 700km to 800km and inclinations of 72°. All satellites, except satellite FM3 have been operational since launch in 2006. Satellite FM3 experienced power issues in 2010 and is no longer operational. COSMIC and GRACE data are available from the COSMIC Data Analysis and Archive Center (CDAAC) database at http://cdaac-www.cosmic.ucar.edu/.

LEO satellites determine electron density profiles up to their orbit altitude using occulting GPS TEC measurements with the Abel inversion technique [Schreiner et al., 1999]. The revised procedure of Pedatella et al. [2015] was used for the COSMIC and GRACE observations. These techniques can be susceptible to the effect of horizontal ionospheric gradients, which can be exacerbated at high latitudes [Pedatella et al., 2015]. To accommodate the limitations of LEO RO electron density observations, quality control of these datasets was undertaken in a manner similar to that of Shubin et al. [2013]. In addition to these quality control measures, we have also omitted profiles where the horizontal track of tangent points is longer than three times the vertical extent of the profile and profiles where negative electron densities are found above 100km altitude. ~735,000 profiles were identified for use in fitting the topside model.

2.3 Topside Sounder

Topside sounders are satellite-mounted, downward-facing ionosondes that provide topside electron density profiles down to the F2-peak altitude (hmF2) [Bilitza et al., 2003]. For this study, we make use of all available topside sounder profiles from above 45°N geomagnetic latitude. The missions included in this dataset are the Alouette 1 and 2 missions, the International Satellites for Ionospheric Studies (ISIS) 1 and 2 missions, and the Intercosmos-19 (IK-19) mission. Information about the orbit, operational period, and number of profiles included in this study are presented in Table 1.

Table 1. *Summary of the characteristics of the topside sounder missions used in this study.*

Mission	Number of Profiles	Operational Period	Orbit Altitude (km)	Orbit Inclination (°)	Orbital Period
Alouette 1 (a,b,c)	3806, 15250, 16584	1962 - 1971	1000	80	~105min
Alouette 2	3768	1965 - 1972	500 - 3000	80	~120min
ISIS 1	7974	1969 - 1980	500 - 3500	88	~130min
ISIS 2	28732	1971 - 1979	1400	88	~115min
IK-19	400	1979 - 1982	500 - 995	74	~100min

For the Alouette and ISIS data, only data that was manually interpreted by the Canadian Communications Research Center (CRC) and had a quality control index better than five were included in the model fitting. The Alouette and ISIS data are available at https://spdf.sci.gsfc.nasa.gov/pub/data/ and the IK-19 data is available at http://www.izmiran.ru/projects/IK19/. Overall, ~77,000 topside sounder profiles were included in the fitting of the topside model.

Contours of measurement density are superimposed over the ISR location map in Figure 2. The number of measurements is presented in 2^{o} x 2^{o} bins.

3 Limitations of the Current NeQuick Topside Model and its Parameterization

Using the data listed in Section 2, we here present an evaluation of the performance of the NeQuick topside model, both in terms of its ability to correctly model the H_o scale height and its ability to properly capture the curvature of the topside electron density profile.

3.1 H_o parameterization

The variable component of the NeQuick topside model is its H_o parameter, given by Equations (4) – (7). To assess the performance of this parameterization, we have fitted the entirety of the dataset from Section 2 to the NeQuick topside model (Equations 1-3) in terms of H_o using non-linear least squares. In this way, we have derived H_o for each profile. We then calculated the expected H_o from Equations (4) – (7) using CCIR foF2 and M(3000)F2, as well as hmF2 from IRI2007. The use of this older hmF2 parameterization is to remain consistent with the hmF2 model used in the original fitting of the NeQuick topside model. This hmF2 should be consistent with that in the NeQuick, which also uses a Bradley-Dudney-type hmF2 parameterization [Nava et al., 2008; Bilitza et al., 1979]. Given the IRI's transition away from Bradley-Dudeney-type hmF2 models to new, standalone, hmF2 models (beginning in IRI2016), it is expected that there may be some inconsistencies in its use of the NeQuick topside model. That however, is a topic for a different study and goes beyond the scope of the current work.

Calculating H_o in this way, we present a comparison between measurement-derived and NeQuick-modeled H_o at various local times throughout the period of study. In Figure 3, we present monthly median measurement-derived and IRI/NeQuick-derived H_o at several different local times. This figure demonstrates some significant issues in the current NeQuick H_o parameterization: 1) a tendency for the model to underestimate the amplitude of solar cycle variability, resulting in underestimation at high solar activity by as much as 60km, and 2) a tendency to underestimate month-to-month variability, particularly during the nighttime. While solar cycle variations are easy to extract from this figure, the sheer extent of the dataset does not allow for an easy interpretation of the smaller-scale variations, such as seasonal variations.

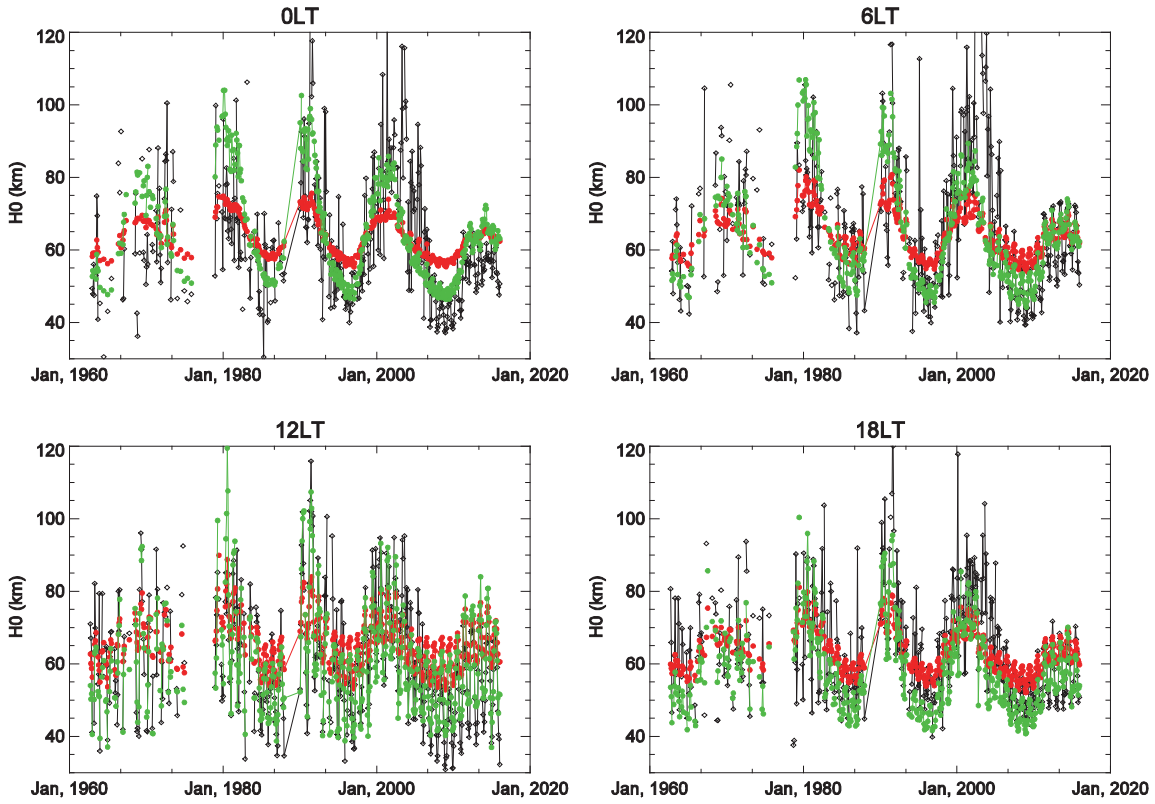

Figure 3. *Plots of monthly median Ho derived from measurements (black), from the traditional IRI/NeQuick (red), and from refitting the NeQuick k parameterization (green) for 00LT, 06LT, 12LT, and 18LT local time hours.*

For the purpose of identifying features at shorter time-scales, we present a subset of the time range of Figure 3, namely from 2007 to 2016, in Figure 4 along with plots of the associated monthly RMS errors. It should be noted that the relatively weak solar maximum of this cycle (2012 - 2015) corresponds to the IRI/NeQuick's best performing solar maximum. Similarly, the anomalously weak solar minimum of this cycle (2007 - 2010) corresponds to the IRI/NeQuick's worst performing solar minimum. Based on this, the following evaluations during this period should be taken as a best-case scenario during solar maximum and a sort of worst case scenario at solar minimum. In Figure 4, we can more easily identify the solar activity and seasonal issues seen in Figure 3. More specifically, we see significantly damped seasonal variability in IRI/NeQuick-derived H_o at all local times, with an almost complete lack of seasonal variability during midnight periods, despite ~10km seasonal variations in the measured values. At all local times, the IRI almost universally overestimates monthly median H_o, sometimes by as much as 25km. The exception to this is good agreement during solar maximum summer, particularly during dawn and dusk periods; however, given the results of Figure 3, this is likely limited to the relatively weak solar maximum of cycle 24, where stronger solar maxima see significant underestimation by the IRI/NeQuick-generated values.

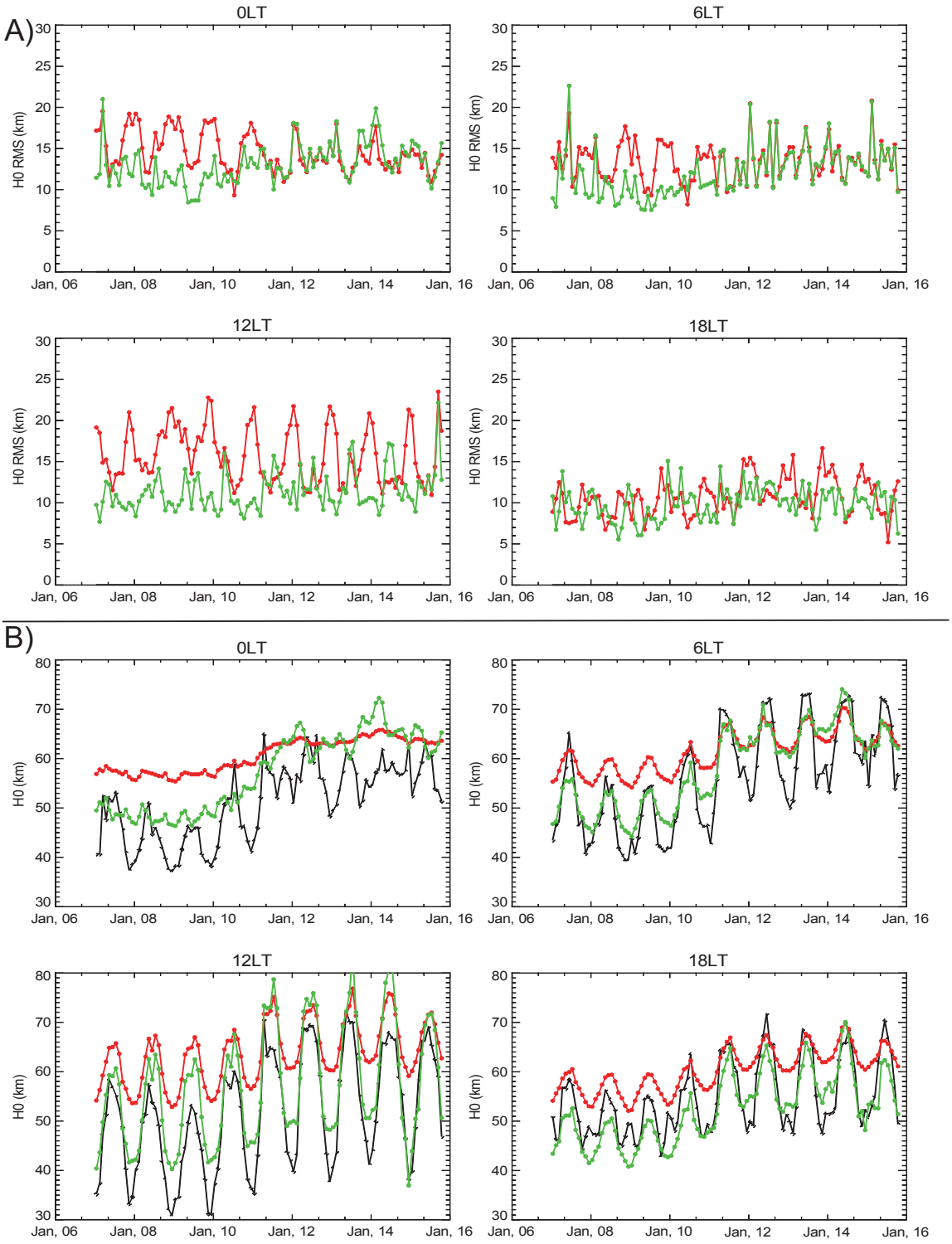

Figure 4. *A) Plots of monthly RMS Ho errors for the traditional IRI/NeQuick (red) and for the refitted NeQuick k parameterization (green) for 00LT, 06LT, 12LT, and 18LT local time hours between 2007 and 2016. B) Same as Figure 3, but only for 2007-2016.*

The distribution of the observed model-derived errors is also presented in Figure 5a. From this figure, we see an overall tendency for the model to overestimate H_o by a median of 7.8km with lower quartile of -0.86km and upper quartile of 15.2km. The distribution also appears to be somewhat skewed toward large underestimation of H_o, possibly associated with the observed strong negative trend in geomagnetic activity errors.

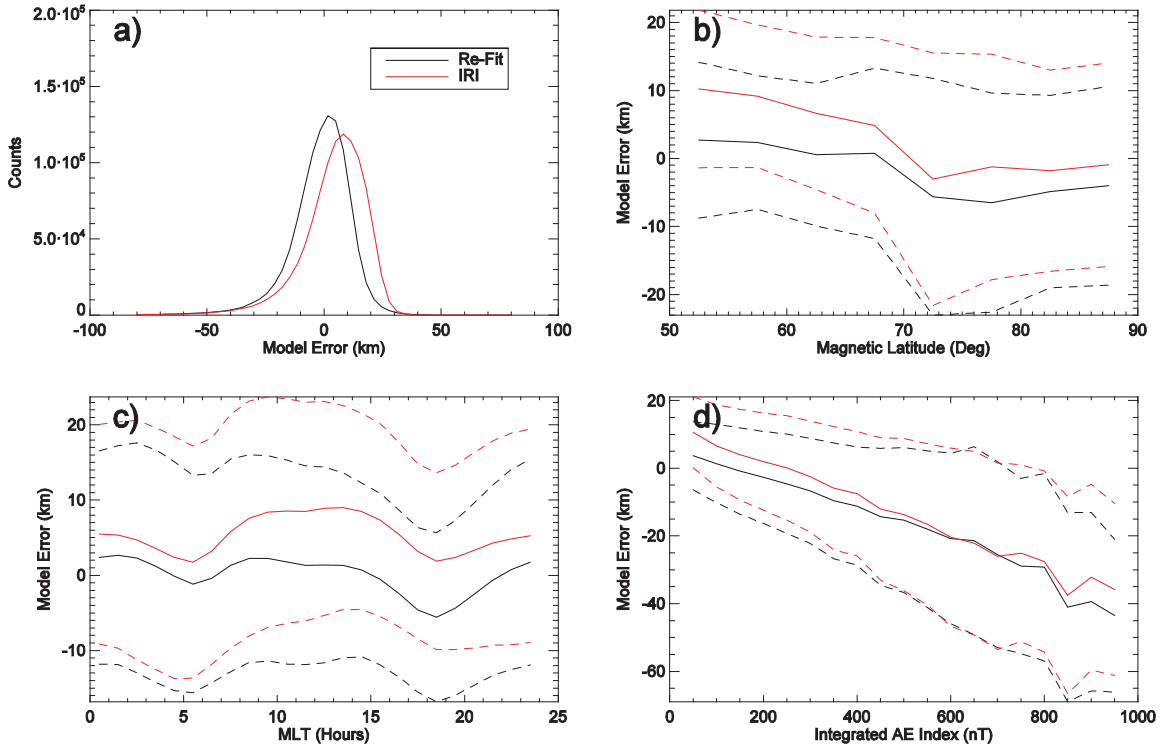

Figure 5. *a) Distributions of Ho differences from measurement-derived values for the traditional IRI/NeQuick (red) and the refitted k parameterization (black). b) Mean (solid) and standard deviation ranges (dashed) of Ho vs. geomagnetic latitude. c) Mean (solid) and standard deviation ranges (dashed) of Ho vs. magnetic local time. d) Mean (solid) and standard deviation ranges (dashed) of Ho vs. integrated AE index.*

To examine the spatial and geomagnetic activity variations of the observed errors in model-derived H_o we have plotted the mean errors with respect to Geomagnetic Latitude, Magnetic Local Time (MLT), and integrated Auroral Electrojet (AE) index in Figure 5. The integrated AE index that is used here is calculated in the same manner as described in Themens et al. [2017a] and follows the methodology of Wu and Wilkinson [1995] and Perrone et al. [2001]. In terms of variations with respect to geomagnetic latitude, we see a tendency for the IRI to overestimate H_o below 70°N by an average of ~10km and standard deviation of ~10km. Above 70°N we see relatively good agreement in the mean, with average underestimation of 0km to 3km; however, standard deviations increase to ~15km. In terms of MLT variability, we see mean overestimation during daytime periods of 8km – 9km with improvements during dawn and dusk periods, which is consistent with our observations from Figure 4. Most interesting in Figure 5 is the observed trend in errors with respect to integrated AE index, where we see a strong linear error trend that reaches an average underestimation of up to 40km at 1000nT. Of course, a median model such as

the IRI/NeQuick should not be expected to be able to represent geomagnetic activity but the linearity of this trend suggests that these errors may be easily corrected through the inclusion of an integrated AE index term in the IRI/NeQuick's H_o parameterization.

3.2 Does H_o need new parameters?

In the previous section, we demonstrated a propensity for significant errors in model-derived H_o, which are consistent with previous studies [e.g. Themens et al., 2014; Themens and Jayachandran, 2016; and Themens et al., 2017b]. The question remains, are these errors a consequence of there being a limited fitting dataset available for the development of the NeQuick model or do they arise from the inability of the parameters in Equation (5) to properly represent the variations in H_o? To assess this, we have re-fitted the NeQuick parameterization of Equation (5) to our entire dataset of H_o. The resulting model is given by the following

$$k = 3.927 - 0.2093foF2 - 0.002979hmF2 - 0.01311\frac{hmF2}{B2_{Bot}} + 0.006925R12 \quad (8)$$

The results of using this new parameterization are presented as the green curves in Figures 3 and 4 and as the black curves in Figure 5. Clearly from these figures, there is a significant improvement in H_o modeled using the re-fitted parameterization. In terms of solar activity variability, we see significantly improved performance during low solar activity periods. Spatially, we see significantly reduced errors at low latitudes. Despite these improvements, we still see significant errors during the winter and an almost complete lack of seasonal variability during nighttime periods. These results demonstrate that the current form of the k parameterization of Equation (5) is insufficient in its capacity to capture the variability of H_o, particularly during nighttime periods. These results suggest that the E-CHAIM topside model, and future versions of the NeQuick, must explore the use of other parameters in their representations of H_o.

3.3 Topside Shape Errors

While limitations in the ability of the model to capture H_o variability are a significant concern, we feel it necessary to examine the suitability of the model function itself (Equations 1-3) in representing the shape of the topside electron density profile. To assess this suitability, we have calculated the differences between IRI-derived electron density profiles and those measured by the various instruments discussed in Section 2. For this, we have generated probability distributions/histograms of the model errors for each altitude above the F-region peak. To ensure that we are solely examining the performance of the topside model, and are not also seeing contamination due to errors in hmF2 or NmF2, we have normalized all of the profiles to NmF2 and used hmF2-relative altitude. In Figure 6 we present contour plots of these error distributions, normalized separately for each altitude. On the left, we plot the distribution of NeQuick model errors, normalized to NmF2 (i.e. $(NeQuick/NmF2 - Measured/NmF2)$). On the right, we have plotted the distribution of relative errors in electron density (i.e. $(NeQuick - Measured)/Measured$). Clearly, from this figure, it is evident that there are appreciable issues in the NeQuick topside electron density representation. In terms of NmF2-relative errors, we see a pattern of significant overestimation in the lower topside, characterized by median overestimation errors of up to 8% of NmF2 and 1-sigma errors of up to 20% of NmF2. At higher altitudes, median errors decrease significantly to within 1% of NmF2 and 1-sigma errors decrease

to ~6% of NmF2; however, the distribution of these errors becomes highly skewed toward underestimation. In terms of relative errors (e.g. Figure 6, right), the situation at high altitudes becomes somewhat concerning, where we see median relative underestimation by 42% at 500km above hmF2. Overall RMS errors for the IRI/NeQuick were found to be 10.34% of NmF2.

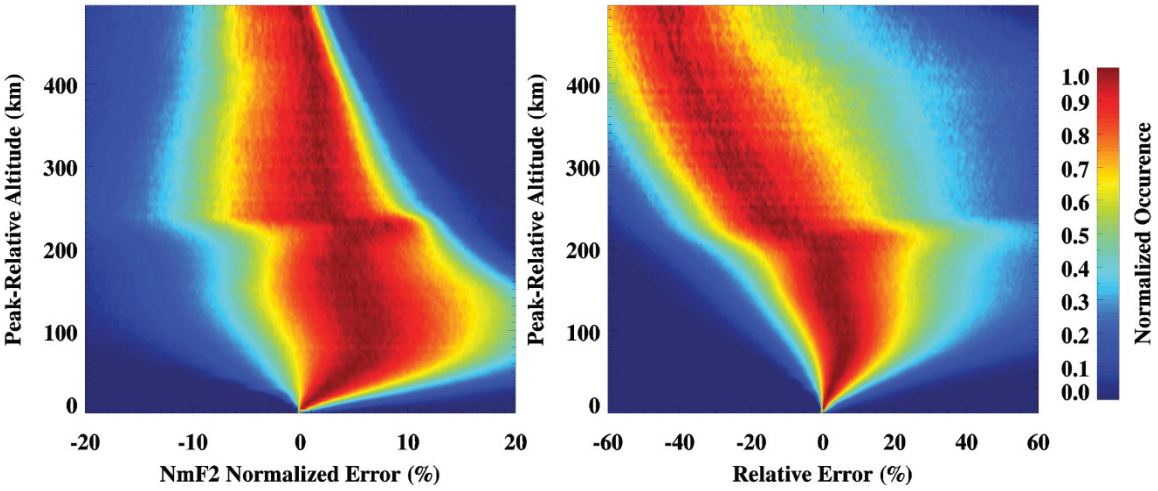

Figure 6. *Left) Normalized distributions of absolute electron density errors, as a percentage of NmF2, vs. altitude for the traditional IRI/NeQuick. Right) Normalized distributions of the corresponding relative errors in electron density vs altitude.*

While the above error distributions provide more insight into the performance of the IRI/NeQuick topside model, they do not provide specific insight into the performance of the shape functions given by Equations (1) – (3). To examine this performance, we present a similar figure to Figure 6, where we now present error distributions for the best-fitted NeQuick profile (fitting only for H_o) in Figure 7. As one would expect, we see significantly reduced distribution spread and somewhat better median errors than the corresponding IRI/NeQuick profiles; however, one can clearly see some remaining issues, namely we still see a trend of overestimation in the lower topside and underestimation at higher altitudes. This is consistent with the results presented in Zhu et al. [2015]. The overall RMS error for this best fit NeQuick model is 4.50 % of NmF2. It should be noted that the discontinuity in the distributions at 200km - 250km is a result of the differences in the sampling ranges of the various instruments used in this study. Below 200km - 250km, the error distribution functions see a significant contribution from ISR observations. Above this altitude there is substantially less ISR data and the dataset is dominated by RO and topside sounder data.

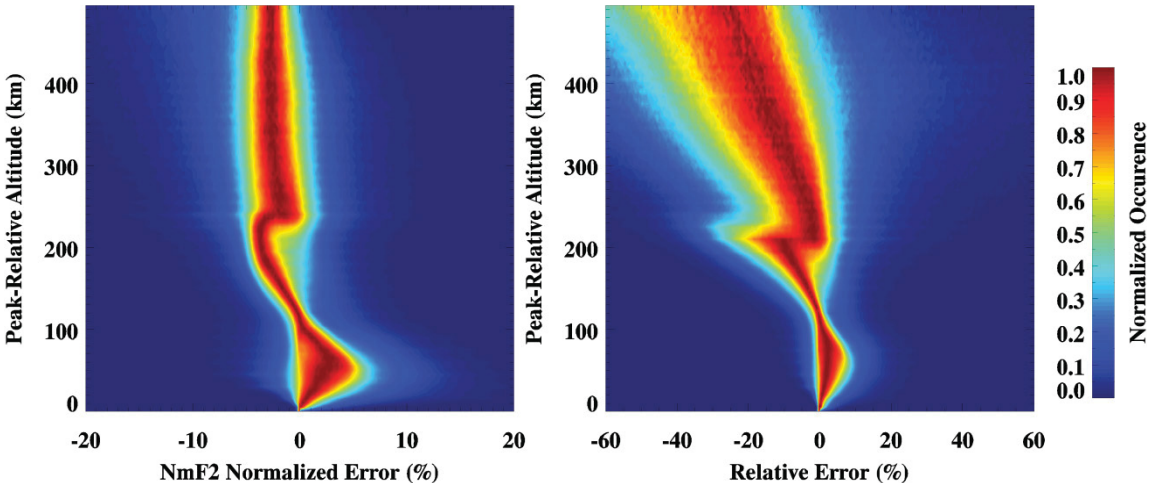

Figure 7. *Same as Figure 6 but for the best-fitted NeQuick parameterization (r,g) = (100,0.125).*

Despite the above issue, this discontinuity can actually provide some measure of insight into the performance of Equations 1 – 3. As we are using least squares, if the model function cannot adequately reflect the shape of the profile to be fitted, the fitting approach will minimize fitting errors by overestimating in one region and underestimating in another (a consequence of only fitting for H_o). In this case, we see overestimation in the near-peak region and underestimation at higher altitudes. For the data with a greater vertical extent, the underestimation and overestimation regions are broader leading to an upward translation of the region of transition between underestimation and overestimation. If the topside model was fully capable of capturing the shape of the topside ionosphere, and the datasets do not exhibit systematic differences from one-another, we would not expect to see such a discontinuity in the error distributions presented in Figure 6. In the following section, we demonstrate this to be the case, assuaging the concern that the datasets may be inconsistent with one-another.

The vertical error trends in Figures 6 and 7, combined with the observed issues in H_o modeling presented in Sections 3.1 and 3.2, demonstrate a need to re-examine the formulation of the NeQuick topside model, both in terms of the H_0 parameterization and the choice of r and g constants, prior to adopting the model for use by E-CHAIM.

4 A Refitted and Parameterized NeQuick Topside

The errors presented here, and in past studies, suggest a need to re-fit the NeQuick. As a first step to doing so, we first attempt to correct the model shape errors presented in Section 3.3.

4.1 New r and g constants

As the r and g constants of the NeQuick model have not been changed since the original implementation of the model and have not been publicly discussed in the past, we see optimizing these parameters as the main opportunity to correct the observed limitations of the current NeQuick topside shape. As a first step to optimizing these parameters, we have calculated the NmF2-normalized RMS errors for all the available data while varying r in steps of 1.0 and g in steps of 0.01. Similarly, we have also calculated the mean correlation between measured and modeled topside profiles varying through the same values of r and g. The results of these tests are presented in Figure 8, where the X marks the location of the current NeQuick's r and g constants and the + marks the location corresponding to the RMS error minimum and correlation maximum on the corresponding plot. As one can see, there is a modest improvement in NmF2-normalized error and correlation between the current NeQuick and the corresponding minimum/maximum. Despite these being relatively modest improvements, we will later show that these corrections can in fact completely correct the shape errors observed in Section 3.3. The RMS error minimum corresponds to (r,g) = (20,0.20) while the correlation maximum corresponds to (20,0.18). As a second assessment of these parameters, we have set r to 20 and re-fitted the NeQuick parameterization to our entire dataset for H_o and g using nonlinear least squares. The corresponding mean g value from this fitting was found to be g = 0.2024±0.043. For the remainder of this study, the new r and g constants are taken as (r,g) = (20,0.2024).

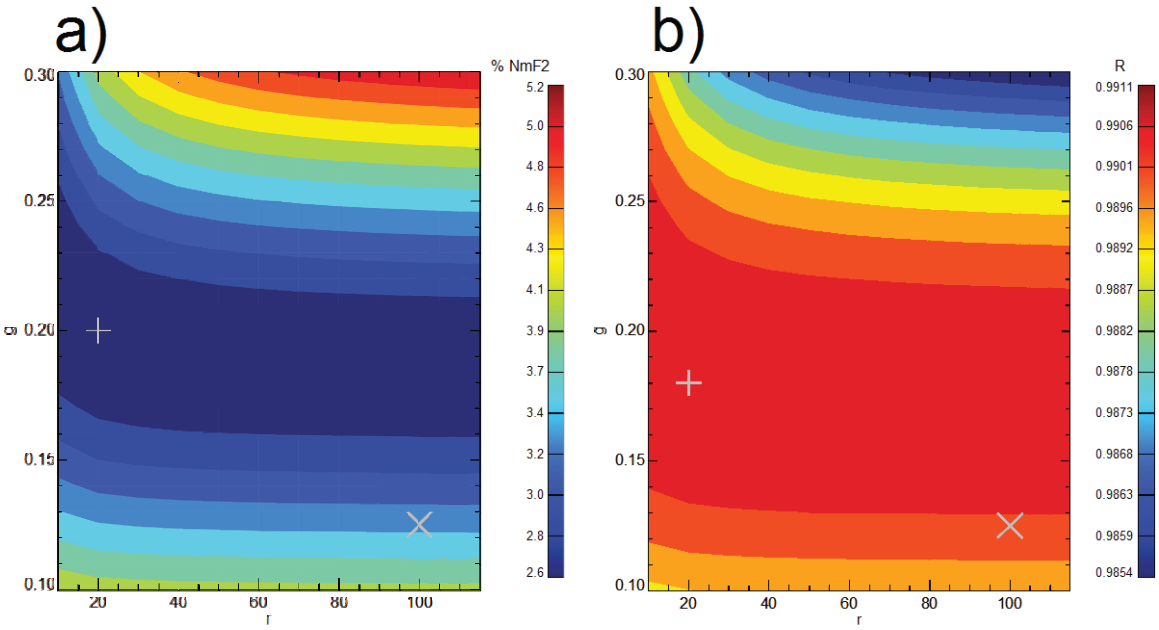

Figure 8. *Contour plots a) of the average NmF2-relative RMS error and b) the average correlation coefficient of best-fitted NeQuick profile functions using varying values of r and g.*

The + marks the corresponding minimum RMS or maximum correlation for each plot. The X marks the values used by the traditional NeQuick model.

Revisiting Figure 1, we see that the traditional NeQuick model's (r,g) of (100,0.125) results in a scale height that remains within 10% of the linear case up to 6000km above the F-region peak. As the data used in fitting these models generally comes from below 2500km above the F-region peak, the traditional parameterization would imply that only a linear scale height variation with altitude with a single constant rate of change (g = 0.125) would be necessary to fit the dataset. This does not, in fact, appear to be the case. Examining the red curve of Figure 1, corresponding to the optimized values for (r,g) of (20,0.2024), we see that the new parameterization quickly diverges from linearity at altitudes within the fitting dataset range.

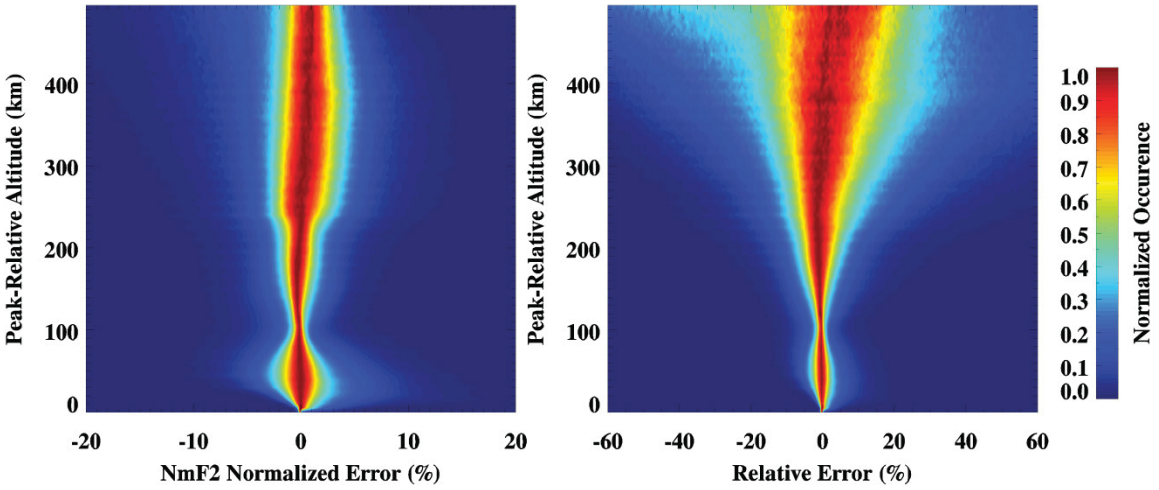

Figure 9. *Same as Figure 6 but for the best-fitted new NeQuick model function using (r,g) = (20,0.2024).*

To assess the performance of these new r and g constants, we have fitted Equations (1) – (3), for H_o, to our dataset using the new r and g constants. In Figure 9 we present error distributions for this best fitted model using new r and g values, similar to Figures 6 and 7. Immediately evident from this figure is the near complete correction of the NeQuick's near-peak overestimation, it's high altitude underestimation, and the discontinuity at the boundary between ISR and RO/topside sounder dominated datasets. The overall RMS error for this new NeQuick model is 3.6% of NmF2. While this is a relatively small improvement, the tendency for the errors of the traditional model to constitute a systematic bias in different altitude regimes makes such an improvement significant nonetheless, particularly when such a model is used as a background or basis set for data assimilation frameworks [Yin and Mitchell, 2014; Bust and Mitchell, 2008] or to calculate the projection shell height for LEO topside TEC observations [Watson et al., 2018].

4.2 Re-fitting H_o for a regional version of the traditional NeQuick

Now that the shape of the topside profile function has been updated/corrected, we may now re-fit the H_o parameterization of Equations (4) and (5). As a baseline, we first re-fit the H_o parameterization to the same parameters as the original NeQuick model (e.g. re-fitting the k

parameterization). The RMS error in H_o for this parameterization was found to be 11.74km. The results of fitting to the traditional parameterization are presented in Figure 10.

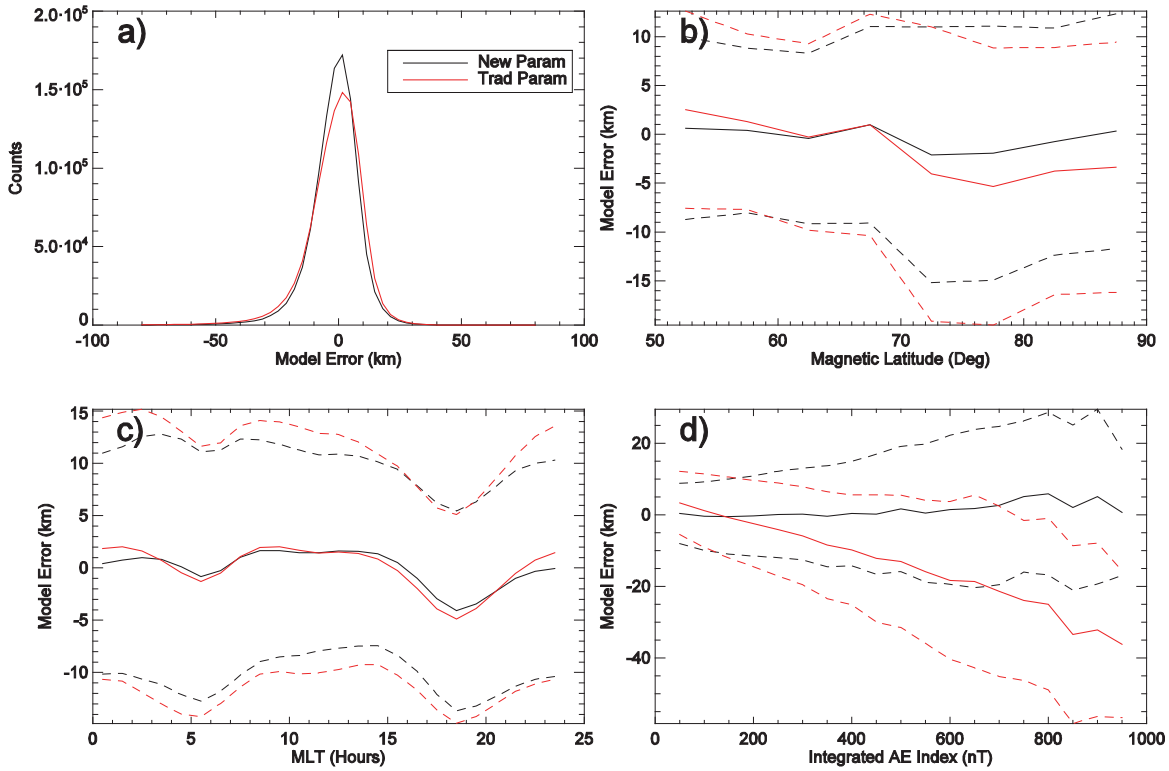

Figure 10. *Same as Figure 5 but the black curves now represent the new Ho parameterization of Equation 9 and the red curves represent the refitted traditional NeQuick k parameterization using the new (r,g) = (20,0.2024).*

Similar to the results from Figure 5, the use of the traditional parameterization of H_o results in an underestimation of H_o at high latitudes, underestimation of H_o during dawn and dusk periods, and a linear pattern of underestimation with respect to geomagnetic activity. To attempt to resolve the observed error patterns, we have made three changes to how H_o is parameterized: 1) we have directly fitted H_o, 2) we have removed all dependence on B2Bot, and 3) we have added additional terms to the parameterization. The new best fitted parameterization is given by the following relationship

$$H_o = 20.120 - 3.734foF2 - 0.0993hmF2 + 0.226R12 + 23.636\cos\chi + 0.639\sin\chi + AE'(0.0691\sin\varphi - 0.0442\cos\varphi) - 1.227\sin\left(\frac{LT\cdot\pi}{12}\right) + 4.821\cos\left(\frac{LT\cdot\pi}{12}\right) \quad (9)$$

where χ is the solar zenith angle, AE' is the integrated AE index, ϕ is the geographic latitude, and LT is the local time. Ap index was also attempted in place of AE in order to retain compatibility with the parameters already within the IRI; however, we found that Ap could not adequately represent the variability of H_0 in very active (Kp 7 or greater) conditions. AE index has previously been assessed as a driver index of F-region ionospheric storm variability in the works

of Wu and Wilkinson [1995] and Perrone et al. [2001], demonstrating comparable performance to other common geomagnetic indices, such as Dst and Ap. At high latitudes, with the dominant ionospheric storm-time response being driven by Joule heating in the vicinity of the auroral electrojets [Yamazaki et al., 2016], AE, as an Auroral Electrojet index, acts as a convenient proxy of this heating. For a potential global re-parameterization of the NeQuick, other indices may be necessary to reflect the different physical processes governing the ionospheric response to storms in different regions of the globe. Nonetheless, clearly from Figure 5, storms generate a strong impact on topside scale thickness and thereby must be accommodated in representations of topside scale thickness, at least at high latitudes.

The use of geographic latitude and local time instead of their corresponding geomagnetic counterparts was to accommodate the limitations of consistently available parameters within the NeQuick and IRI models. RMS errors for this newly fitted H_o model were found to be 10.18km. We have chosen to refit H_o directly here for several reasons: 1) fitting H_o directly resulted in slightly lower RMS errors than re-fitting k with the same parameterization, and 2) as mentioned in Themens et al. [2017b] using improved B2Bot can have a negative impact on the performance of H_o parameterizations; thus, fitting H_o directly will reduce the impact of significant B2Bot errors and new B2Bot parameterizations, such as that of Alazo-Cuartas and Radicella [2017], on the topside model.

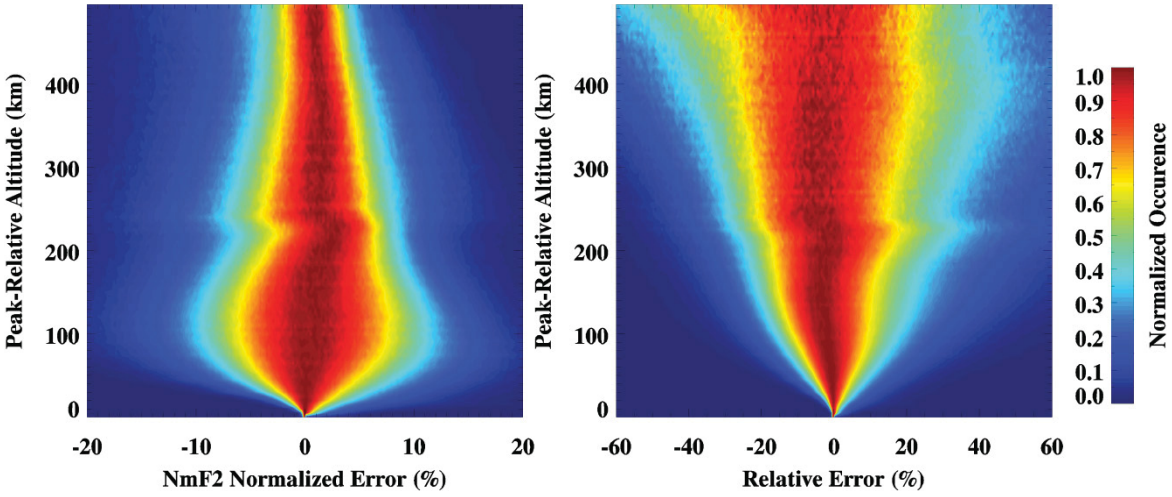

Figure 11. *Same as Figure 6 but for the new NeQuick parameterization of Equation 9 with (r,g) = (20,0.2024).*

The performance of this new H_o parameterization is presented as the black curves in Figure 10. Clearly, the resulting H_o exhibits virtually no mean errors in latitude, reduced mean errors in MLT variability, and only marginal mean errors with increasing geomagnetic activity. In Figure 11, we present error distributions for each altitude using the new parameterization. This figure demonstrates a significant improvement over the original results of the IRI that were presented in Figure 6. Median NmF2-normalized errors remain below 3% of NmF2 at all altitudes with 1-sigma errors consistently below 10% of NmF2. Overall RMS errors were found to be 7.16% of NmF2. It should be noted that this is a regional alternative parameterization for the NeQuick topside and should not be used in regions below 50^{o}N geomagnetic latitude; however, we hope

that the improvement seen through our changes to the parameterization will assist the NeQuick team in their development of the next generation global topside NeQuick model.

4.3 A Topside for E-CHAIM

Based on the results of Sections 4.1 and 4.2, we may now propose a topside model for E-CHAIM; unfortunately, the inavailability of M(3000)F2 in the E-CHAIM model necessitates that we not use the parameterization of Section 4.2 and instead develop a stand-alone parameterization for E-CHAIM.

The E-CHAIM, first introduced in Themens et al. (2017a), is an empirical representation of ionospheric electron density above 45°N geomagnetic latitude. The model is composed of separate models for the each of hmF2, NmF2, topside vertical shape, and bottomside vertical shape. Each of these models is built around a spherical cap harmonic expansion in Altitude Adjusted Corrected Geomagnetic (AACGM) coordinates for horizontal spatial variability, a Fourier expansion for seasonal variability, and a function of F10.7 cm solar radio flux for solar cycle variability. As we are here developing a topside model for sole use with E-CHAIM, we have increased flexibility in the number and type of parameters available for use with the model, as compared to what is available when were redeveloping the topside model to be used with both the NeQuick and IRI. It is also our intent to develop a topside model not dependent on ionospheric characteristics, such as hmF2 and foF2, so that future updates of models for those characteristics will not affect other components of E-CHAIM. Taking advantage of the above stated flexibility and avoiding the use of ionospheric characteristic terms, we propose the following model of a similar form to that used for the other components of E-CHAIM:

$$H_0 = G + \sum_{l=0}^{L}\sum_{m=0}^{\min(l,M)}\left[A_{lm}\cos\left(\frac{\pi m}{180}MLT\right) + B_{lm}\sin\left(\frac{\pi m}{180}MLT\right)\right]P_{lm}(\eta) \quad (10)$$

$$A_{lm}, B_{lm} = (\gamma_{lm}F_1 + \delta_{lm}F_2)\cdot sin^2\left(\frac{\pi\cdot DoY}{365.25}\right) + (C_{lm}F_1 + D_{lm}F_2) \quad (11)$$

$$C_{lm}, D_{lm} = \sum_{c=1}^{4}\alpha_{lm}^{c}\cos\left(\frac{2\pi c\cdot DoY}{365.25}\right) + \beta_{lm}^{c}\sin\left(\frac{2\pi c\cdot DoY}{365.25}\right) \quad (12)$$

$$\mathrm{G} = F10.7\cdot(a_1\cos(\chi) + a_2\sin(\chi)) + \sqrt{F10.7}\cdot(a_3\cos(\chi) + a_4\sin(\chi)) + a_5\cos(\chi) + a_6\sin(\chi) + \sin(\chi)\cdot(a_7\sin\theta + a_8\cos\theta) + \cos(\chi)\cdot(a_9\sin\theta + a_{10}\cos\theta) + a_{11}\sin\theta + a_{12}\cos\theta \quad (13)$$

where *MLT* is AACGM local time, *L* = 5, *M* = 5, *F1* is 81-day smoothed F10.7 flux, *F2* is integrated AE index, *DoY* is the day of year, θ is the dipole tilt angle, χ is the solar zenith angle, $a_{1\text{-}12}$, α_{lm}^{c}, β_{lm}^{c}, γ_{lm}, and δ_{lm} are fitting coefficients, and

$$\eta = \cos\left((90 - \varphi)\frac{\pi}{45}\right) \quad (14)$$

where φ is AACGM latitude. MLT is used for the longitudinal coordinate to account for the limited spatial coverage of the available data set in a similar manner to Altadill et al. (2013). The

solar zenith angle terms partially accommodate for the short comings of this type of parameterization in representing UTC-dependent variations. RMS errors in H_0 using this parameterization are 9.05km. Overall RMS errors in electron density are 6.62% of NmF2. A comparison of the performance of this H_0 parameterization with respect to that of Equation 9 is presented in Figure 12 in a similar manner as used in Figures 5 and 10. Clearly, there are slight improvements in the use of the E-CHAIM parameterization over the new NeQuick parameterization, particularly with respect to diurnal variations, likely attributed to variations better represented via a geomagnetic coordinate system, and at high latitudes. Biases in modeled H_0 are shown to remain within 1km in MLT and MLat. Biases only exceed 1km in conditions with integrated AE index above 700nT and never exceed 5km.

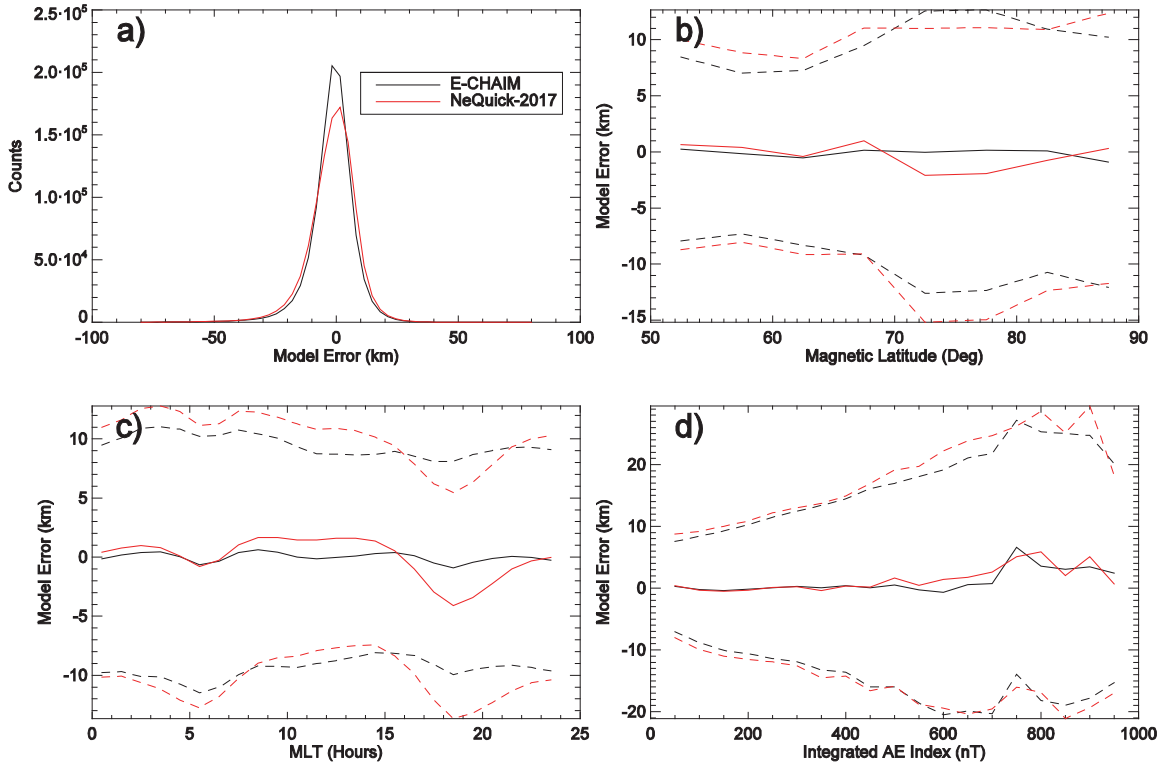

Figure 12. *Same as Figure 10 but for H0 derived from the E-CHAIM parameterization (black) and that of Equation 9 (red).*

5 Conclusion

We have here diagnosed shortcomings in the NeQuick topside model and its parameterization at high and upper-mid latitudes, showing that not only are there errors in the NeQuick's modeling of the monthly median topside scale height by up to 60 km, but that there are also fundamental concerns regarding the shape of the topside model itself. Building upon these results, we have then shown that the use of a very limited set of parameters to fit the k parameter of the NeQuick model results in errors, particularly at nighttime, that cannot be resolved even when re-fitting the traditional NeQuick Ho parameterization.

These results led us to first update the r and g constants of the NeQuick model to 20 and 0.2024, respectively. This resulted in a substantial improvement in the NeQuick model's ability to fit the observed topside electron density profiles, exhibiting no significant mean errors at all altitudes. Following this, we estimated Ho for this new NeQuick model and fitted the resulting data to various parameterizations including: 1) the traditional NeQuick parameterization, where the k parameterization was refit, 2) a new parameterization that directly models Ho using the original NeQuick parameters, as well as AE index, solar zenith angle, and local time terms, and 3) a newly proposed E-CHAIM parameterization. RMS errors using these approaches each represented a significant improvement over the traditional IRI/NeQuick topside model with NmF2-normalized mean errors of 0.70%, 0.66%, and 0.65% of NmF2, respectively, and RMS errors of 8.03%, 7.16%, and 6.62% of NmF2, respectively, compared to the traditional IRI/NeQuick's corresponding mean error of 3.56% and RMS error of 10.34% of NmF2. Based on these results, we recommend that users consider the use of Equation (9) with the IRI and NeQuick in regions above 50oN geomagnetic latitude or consider the use of the E-CHAIM topside model in these regions.

Future work in optimizing the NeQuick parameterization and building an updated global topside model should examine re-fitting the r and g constants in restricted latitude domains or examine the feasibility of replacing these constants with parameterizations, as r strongly controls the scale height at high altitudes and g controls the rate of change of the scale height, which will be characteristically different for different latitudes, local times, solar activity levels, and geomagnetic activity conditions. The challenge in this will be ensuring that the errors due to modeling additional parameters are not so large as to negate the potential improvement in their ability to capture the variations of the topside profile shape. We ultimately hope that this study provides the developers of the NeQuick with some ideas for the future development of what has been a very successful topside model so far. Validation of the proposed models will be conducted in a future study using an independent dataset of radio occultation measurements. In the interim, we invite the community to validate our proposed models and suggest potential improvements.

References/Bibliography

Alazo-Cuartas, K., and S.M. Radicella (2017), An improved empirical formulation of an ionosphere bottomside electron density profile thickness parameter, *Adv. Space Res.*, doi:10.1016/j.asr.2017.06.030

Altadill, D., S. Magdaleno, J.M. Torta, and E. Blanch (2013), Global empirical models of the density peak height and of the equivalent scale height for quiet conditions, *Adv. Space Res.*, 52, 1756-1769, doi:10.1016/j.asr.2012.11.018

Bilitza, D., N. M. Sheikh, and R. Eyfrig (1979), A global model for the height of the F2-peak using M3000 values from the CCIR numerical map, *Telecommun. J.*, 46, 549–553.

Bjoland, L.M., V. Belyey, U.P. Lovhaug, and C. La Hoz (2016), An evaluation of International Reference Ionosphere electron density in the polar cap and cusp using EISCAT Svalbard radar measurements. *Ann. Geophys.*, 34, 751-758, doi:10.5194/angeo-34-751-2016

Bust, G. S., and C. N. Mitchell (2008), History, current state, and future directions of ionospheric imaging, *Rev. Geophys.*, 46, RG1003, doi:10.1029/2006RG000212

Coïsson, P., S.M. Radicella, R. Leitinger, and B. Nava (2006). Topside electron density in IRI and NeQuick: Features and limitations. Adv. Space Res., 37, pp. 937-942.

Evans, J. (1969), Theory and practice of ionosphere study by Thomson scatter radar, *Proc. IEEE*, 57 (4), 496–530.

Gordiyenko, G.I., and A.F. Yakovets (2017), Comparison of midlatitude ionospheric F region peak parameters and topside Ne profiles from IRI2012 model prediction with ground-based ionosonde and Alouette II observations, *Adv. Space Res.*, 60(2), 461-474, doi:10.1016/j.asr.2017.01.006

Nava, B., P. Coïsson, and S.M. Radicella (2008), A new version of the NeQuick ionosphere electron density model. *J. Atmos. and Solar-Terr. Phys.*, 70(15), 1856-1862 doi:10.1016/j.jastp.2008.01.015

Pedatella, N. M., X. Yue, and W. S. Schreiner (2015), An improved inversion for FORMOSAT-3/COSMIC ionosphere electron density profiles*, J. Geophys. Res. Space Physics*, 120, 8942–8953, doi:10.1002/2015JA021704.

Perrone, L., G. De Franceschi, and T.L. Gulyaeva (2001). The time-weighted magnetic indices ap, PC, AE, and their correlation to the southern high latitude ionosphere, *Phys. Chem. Earth*, 26(5), 331-334

Radicella, S.M. and R. Leitinger (2001): The Evolution of the DGR Approach to Model Electron Density Profiles, *Adv. Space Res.*, 27 (1), 35-40.

Radicella, S.M. and M.L. Zhang (1995), The improved DGR analytical model of electron density height profile and total electron content in the ionosphere, *Annali di Geofisica*, 38(1), 35-41.

Schreiner, W. S., S. V. Sokolovskiy, C. Rocken, and D. C. Hunt (1999), Analysis and validation of GPS/MET radio occultation data in the ionosphere, Radio Sci., 34(4), 949–966, doi:10.1029/1999RS900034.

Shubin, V.N., A.T. Karpachev, and K.G. Tsybulya (2013) Global model of the F2 layer peak height for low solar activity based on radio-occultation data, *J. Atm. Sol.-Ter. Phys.*, 104, 106-115, doi:10.1016/j.jastp.2013.08.024

Themens, D. R., P. T. Jayachandran, M. J. Nicolls, and J. W. MacDougall (2014), A top to bottom evaluation of IRI 2007 within the polar cap, *J. Geophys. Res. Space Physics*, 119, 6689–6703, doi:10.1002/2014JA020052.

Themens, D.R., and P.T. Jayachandran (2016), Solar activity variability in the IRI at high latitudes: Comparisons with GPS total electron content. *J. Geophys. Res. Space Physics*, 121, doi:10.1002/2016JA022664.

Themens, D.R., P.T. Jayachandran, I. Galkin, and C. Hall (2017a). The Empirical Canadian High Arctic Ionospheric Model (E-CHAIM): NmF2 and hmF2, *J. Geophys. Res. Space Physics*, doi: 10.1002/2017JA024398

Themens, D.R., P.T. Jayachandran, and R.H. Varney (2017b), Examining the use of the NeQuick bottomside and topside parameterizations at high latitudes, *Adv. Space Res.*, doi: 10.1016/j.asr.2017.09.037

Watson, C., Langley, R. B., Themens, D. R., Yau, A. W., Howarth, A. D. & Jayachandran, P. T. (2018). Enhanced Polar Outflow Probe (e-POP) ionospheric radio occultation measurements at high latitudes: Receiver bias estimation and comparison with ground-based observations. *Radio Science*, 53. https://doi.org/10.1002/2017RS006453

Wu, J., and P.J. Wilkinson (1995). Time-weighted magnetic indices as predictors of ionospheric behaviour, *J. Atmos. and Solar-Terr. Phys.*, 57(14), 1763-1770

Xiong, C., H. Lühr, and S.Y. Ma (2013), The subauroral electron density trough: Comparison between satellite observations and IRI-2007 model estimates, *Adv. Space Res.*, 51, 536-544, doi:10.1016/j.asr.2011.09.021

Y. Yamazaki, M.J. Kosch, Y. Ogawa, D.R. Themens (2016), High-latitude ion temperature climatology during the International Polar Year 2007–2008, *Journal of Space Weather and Space Climate*, 6, A35

Yin, P., and C. N. Mitchell (2014), Improving the vertical electron density profile in ionospheric imaging at storm time: A case study on 25–27 September 2011, *J. Geophys. Res. Space Physics*, 119 ,7963–7971, doi:10.1002/2014JA019899

Zhu, J., B. Zhao, W. Wan, B. Ning, and S. Zhang (2015), A new topside profiler based on Alouette/ISIS topside sounding, *Adv. Space Res.*, 56, 2080-2090, doi:10.1016/j.asr.2015.08.008

This page intentionally left blank.

List of symbols/abbreviations/acronyms/initialisms

DND	Department of National Defence
E-CHAIM	Empirical Canadian High Arctic Ionospheric Model
IRI	International Reference Ionosphere
NmF2	Peak density of the F2-layer
hmF2	Height of the F2-layer peak
foF2	The F2-layer critical frequency
M3000F2	Ratio of the MUF to foF2
MUF(3000)	Maximum Usable Frequency at 3000km distance
CHAIN	Canadian High Arctic Ionospheric Network
IRTAM	IRI-based Real-Time Assimilative Model
GIRO	Global Ionospheric Radio Observatory
MIT	Main Ionospheric Trough
DRDC	Defence Research and Development Canada
DSTKIM	Director Science and Technology Knowledge and Information Management

DOCUMENT CONTROL DATA

*Security markings for the title, authors, abstract and keywords must be entered when the document is sensitive

1. ORIGINATOR (Name and address of the organization preparing the document. A DRDC Centre sponsoring a contractor's report, or tasking agency, is entered in Section 8.)

University of New Brunswick
8 Bailey Drive
P.O. Box 4400
Fredericton (New Brunswick) E3B 5A3
Canada

2a. SECURITY MARKING (Overall security marking of the document including special supplemental markings if applicable.)

CAN UNCLASSIFIED

2b. CONTROLLED GOODS

NON-CONTROLLED GOODS
DMC A

3. TITLE (The document title and sub-title as indicated on the title page.)

The Empirical Canadian High Arctic Ionospheric Model (E-CHAIM): Topside

4. AUTHORS (Last name, followed by initials – ranks, titles, etc., not to be used)

Themens, D.; Jayachandran, P.T.; McCaffrey, A.; Reid, B.

5. DATE OF PUBLICATION (Month and year of publication of document.)	6a. NO. OF PAGES (Total pages, including Annexes, excluding DCD, covering and verso pages.)	6b. NO. OF REFS (Total references cited.)
March 2018	24	25

7. DOCUMENT CATEGORY (e.g., Scientific Report, Contract Report, Scientific Letter.)

Contract Report

8. SPONSORING CENTRE (The name and address of the department project office or laboratory sponsoring the research and development.)

Corporate Office
ADM(S&T) / DRDC Corporate
NDHQ (Carling), 60 Moodie Drive, Building 7
Ottawa, Ontario K1A 0K2
Canada

9a. PROJECT OR GRANT NO. (If appropriate, the applicable research and development project or grant number under which the document was written. Please specify whether project or grant.)	9b. CONTRACT NO. (If appropriate, the applicable number under which the document was written.)
03ba - Air Integrated – RF	W7714-186507/001/SS

10a. DRDC PUBLICATION NUMBER (The official document number by which the document is identified by the originating activity. This number must be unique to this document.)	10b. OTHER DOCUMENT NO(s). (Any other numbers which may be assigned this document either by the originator or by the sponsor.)
DRDC-RDDC-2018-C202	

11a. FUTURE DISTRIBUTION WITHIN CANADA (Approval for further dissemination of the document. Security classification must also be considered.)

Public release

11b. FUTURE DISTRIBUTION OUTSIDE CANADA (Approval for further dissemination of the document. Security classification must also be considered.)

12. KEYWORDS, DESCRIPTORS or IDENTIFIERS (Use semi-colon as a delimiter.)

Canadian High Arctic Ionospheric Model; International Reference Ionosphere; oblique ionospheric sounder; High-frequency Radar

13. ABSTRACT/RÉSUMÉ (When available in the document, the French version of the abstract must be included here.)

In this study, we present a topside model representation to be used by the Empirical Canadian High Arctic Ionospheric Model (E-CHAIM). In the process of this, we also present a comprehensive evaluation of the NeQuick's, and by extension the International Reference Ionosphere (IRI)'s, topside electron density model for mid and high latitudes in the northern hemisphere. Using data gathered from all available Incoherent Scatter Radars, Topside Sounders, and GNSS Radio Occultation satellites, we show that the current NeQuick parameterization suboptimally represents the shape of the topside electron density profile at these latitudes and performs poorly in the representation of seasonal and solar cycle variations of the topside scale thickness. Despite this, the simple, one-variable, NeQuick model is a powerful tool for modeling the topside ionosphere. By refitting the parameters that define the maximum topside scale thickness and the rate of increase of the scale height within the NeQuick topside model function, rand g, respectively, as well as refitting the model's parameterization of the scale height at the Fregion peak, Ho, we find considerable improvement in the NeQuick's ability to represent the topside shape and behaviour. Building on these results we present a new topside model extension of the E-CHAIM based on the revised NeQuick function. Overall RMS errors in topside electron density are improved over the traditional IRI/NeQuick topside by 31% for a new NeQuick parameterization and by 36% for a newly proposed topside for E-CHAIM.

Dans cette étude, nous présentons une représentation des couches supérieures qui pourra être utilisée par l'Empirical Canadian High Arctic Ionospheric Model (E-CHAIM), modèle empirique ionosphérique de l'Extrême-Arctique canadien. Dans le même élan, nous présentons aussi une évaluation approfondie du modèle de densité des électrons des couches supérieures NeQuick, et par extension de l'initiative International Reference Ionosphere (IRI), pour les latitudes moyennes à élevées dans l'hémisphère nord. Au moyen de données recueillies par tous les radars à diffusion incohérente, satellites de sondage en altitude et satellites de radio-occultation du GNSS disponibles, nous montrons que le paramétrage actuel de NeQuick représente de manière sous-optimale la forme du profil de densité des électrons des couches supérieures à ces latitudes et qu'elle représente médiocrement les variations saisonnières et liées au cycle solaire de l'épaisseur d'échelle en altitude. Malgré cela, le modèle NeQuick, simple et à variable unique, est un outil puissant pour modéliser la couche supérieure de l'ionosphère. En réajustant les paramètres qui définissent l'épaisseur d'échelle en altitude, et le taux d'augmentation de la hauteur d'échelle dans la fonction de modélisation de NeQuick, r et g, respectivement, ainsi qu'en réajustant le paramétrage du modèle pour la hauteur d'échelle au sommet de la région F, Ho, nous obtenons une nette amélioration de la capacité de NeQuick de représenter la forme et le comportement de la couche supérieure. En nous basant sur ces résultats, nous présentons une nouvelle extension du modèle pour les couches supérieures d'E-CHAIM, d'après la fonction révisée de NeQuick. Les erreurs quadratiques moyennes globales dans la densité des électrons de la couche supérieure sont améliorées par rapport au modèle traditionnel IRI/NeQuick, de 31% pour un nouveau paramétrage de NeQuick, et de 36% pour une nouvelle couche supérieure pour E-CHAIM.